Derated Mode of Power Generation in PV System Using Modified Perturb and Observe MPPT Algorithm

Vinit Kumar and Mukesh Singh

***Abstract*—In a grid-integrated photovoltaic system (GIPVS), there exist issues such as surplus active power and inadequate performance of maximum power point tracking (MPPT). A surplus active power causes the overvoltage problem at the point of common coupling in low- or medium-voltage grid during the peak hours of power generation. Additionally, the inadequate performance of the MPPT algorithm results in power loss due to high settling time during the sudden change of irradiance. Therefore, to solve the surplus power problem, the curtailment of active power is suggested with improved MPPT algorithm under variable irradiance conditions. In this paper, a derated power generation mode (DPGM) control strategy is presented for the curtailment of active power. Additionally, a drift-free (named as modified) perturb and observe (P&O) technique is also proposed to improve the performance of the MPPT algorithm. Consequently, the DPGM control scheme with the intermediate boost converter shaves the surplus active power during the peak hours of power generation. Furthermore, the modified MPPT algorithm deals with the fluctuation of irradiance during non-peak hours. Thus, the proposed control scheme delivers in a more efficient system during the peak hours of power generation. In addition, it reduces the power loss and settling time during the change of irradiance for non-peak hours. Based on the proposed control scheme, a 30 kW system has been simulated in MATLAB/Simulink using Simpower tools under different environmental conditions.**

***Index Terms*—Derated power generation mode (DPGM), grid-integrated photovoltaic system, intermediate boost converter, modified perturb and observe, voltage source inverter.**

NOMENCLATURE

ΔD	Step size of duty ratio
ΔP_{PV}	Change in photovoltaic (PV) power
ΔT	Temperature difference between actual and standard test condition (STC)
ΔV_{PV}	Change in PV voltage
ω	Angular frequency of grid voltage
C_{in}	Input capacitor
C_{out}	Direct current (DC)-link capacitor
D	Duty ratio for boost converter
G	Operating solar irradiance
G_n	Reference solar irradiance
I_d^*, I_q^*	d-axis and q-axis reference currents of inverter
I_d, I_q	d-axis and q-axis currents of inverter
I_o	Reverse saturation current of diode
I_a, I_b, I_c	Grid-side three-phase currents of grid-intigrated PV system
I_{DC}	Output current of boost converter
I_{MPP}	Current at maximum power point
I_{PV}	Current of PV array
I_{scn}	Short-circuit current of PV array at STC
I_{sc}	Short-circuit current of PV array
k_i	Temperature coefficient
L	Interfacing inductor at output of inverter
m_d, m_q	d-axis and q-axis modulation indexes for inverter
N_p	Number of PV modules in parallel
N_s	Number of PV modules in series
$P(t_9\text{-}t_{16})$	Power generated from PV source in particular hours of day
P_{DC}	Output power of boost converter
P_{limit}	Power transfer limit
P_{MPP}	Power at maximum power point (MPP)
P_{peak}	Maximum generated power
P_{PV}	Power of PV array
R	Resistance of each phase
R_{in}	Input impedance of boost converter
R_{out}	Output impedance of boost converter
$S_1\text{-}S_6$	Gate signals for inverter
$t_9\text{-}t_{16}$	Particular hours of day
$t_{s,V_{MPP}}$	Settling time to meet V_{MPP}
$t_{s,V_{DC\text{-}link}^{ref}}$	Settling time to meet $V_{DC\text{-}link}^{ref}$

Manuscript received: April 20, 2019; accepted: May 15, 2020. Date of Cross-Check: May 15, 2020. Date of online publication: September 24, 2020.

This work was supported by the Department of Science and Technology (DST), India (No. DST/CERI/MI/SG/2017/080).

V. Kumar (corresponding author) and M. Singh are with Thapar Institute of Engineering and Technology, Patiala, Punjab, India (e-mail: vinitk72@gmail.com; mukesh.singh@thapar.edu).

DOI: 10.35833/MPCE.2019.000258

V_d^*, V_q^*	d-axis and q-axis reference voltages of inverter
$V_{DC\text{-}link}^{ref}$	Reference DC-link voltage for inverter
V_d, V_q	d-axis and q-axis voltages of inverter
V_t	Thermal voltage of diode
$V_{DC\text{-}link}$	Measured DC-link voltage of inverter
V_{DC}	Output voltage of boost converter
V_{MPP}	Voltage at MPP
V_{PV}	Voltage of PV array
V_{sa}, V_{sb}, V_{sc}	Grid-side voltages of grid-integrated PV system
V_{sd}, V_{sq}	d-axis and q-axis voltages of power grid
V_{ta}, V_{tb}, V_{tc}	Terminal voltages of inverter

I. Introduction

NOWADAYS, the integration of renewable energy sources (RESs) is increasing in power generation due to the shortcoming of fossil fuels. RESs include wind energy, solar energy, hydro energy, fuel cell and tidal energy. Among these RESs, the installation of photovoltaic (PV) solar system is advantageous due to low-cost maintenance. Therefore, the integration of the PV systems is booming in the renewable energy market. However, the PV power generation depends upon the irradiance, which affects the power generation but can be improved by power forecasting [1], [2]. Additionally, the use of PV systems has exponentially increased due to the advancement in power electronic research [3]. PV systems are classified as stand-alone PV, grid-integrated PV and hybrid PV systems. Among these, the grid-integrated PV system (GIPVS) has an advantage over others due to its bulk power transfer capability. However, the GIPVS has some disadvantages such as overvoltage at the point of common coupling (PCC) during surplus power generation. Additionally, the maximum power point tracking (MPPT) algorithm takes more settling time, which causes power loss under variable irradiance condition. These issues affect the smooth functioning of the GIPVS. The effect of high amount of power generation during peak hours is the greatest, which causes overvoltage in the grid. It also affects the safety of equipment in the grid such as transformers, circuit breakers, relays or contactors (for low or high voltage application, respectively) and conductors. In addition, the tracking capability of MPPT algorithms get affected due to the random change of irradiance. These issues impose extra cost when the equipment gets damaged. Therefore, a suitable control approach and the MPPT algorithm are required.

Many researchers have contributed to solving the problems such as overvoltage and inadequate performance of MPPT in GIPVS. Reference [4] presents a generation curtailment technique to prevent the rise of voltage and reverse power flow in the low-voltage distribution network from high penetration of PV power. However, no control technique is recommended to minimize the switching losses and increase the utilization of the inverter. Furthermore, [5] presents a droop-based curtailment approach to protect the grid from overvoltage. Although this scheme increases the power loss compared with normal active power curtailment, it affects the revenue of the system. Similarly, [6] suppresses the power fluctuation of GIPVS using various approaches such as battery storage, dump loads and software-based power curtailment. However, the aforementioned approaches have a high installation cost except power curtailment. Likewise, [7] proposes a reduced power generation mode control algorithm to suppress the output power of the system. It works in reduced power generation mode when generated power exceeds the system rating, although the proposed control strategy fails to reduce the power losses during power curtailment.

Reference [8] proposes a constant power generation scheme to reduce thermal loading, improve the inverter utilization and reduce the switching losses of inverter during rapid irradiance change. However, no appropriate method is presented to decide the power limit. In addition, [9] and [10] present a constant power generation scheme for the overshoot, power loss and active curtailment. The power- or current-based scheme is used in fast dynamic response and MPPT for high robustness, although no other MPPT is used except the perturb and observe (P&O) technique. Similarly, [11] has also proposed a constant power generation scheme for the single-stage and two-stage three-phase GIPVSs. In this scheme, a voltage-based curtailment approach is proposed along with the flexibility of operation points. However, the main shortcoming of this scheme is that it does not suggest any suitable approach to decide the voltage operation point during variable irradiance, although only the conventional MPPT is used to find the operation point.

Therefore, to derate the PV power during peak hours of power generation, the applied control schemes in the aforementioned literature have the following limitations:

1) Most of the existing technologies are based on conventional MPPT (P&O and incremental conductance) techniques.

2) Implemented systems are mostly single-phase GIPVSs.

3) A proper tracking strategy has not been proposed, which can reduce the power loss during the search of maximum power point (MPP).

The aforementioned limitations can be resolved through a proposed derated power generation control scheme with a modified MPPT. The proposed scheme will perform in both peak and non-peak hours of power generation, and improve the tracking capability of the MPPT algorithm. It will resolve the problems such as overvoltage, drifting, oscillation near the MPP, and tracking speed. As a result, the power loss during the search of operation point will be reduced at variable irradiance level. Hence, a suitable MPPT algorithm is required.

Many researchers have classified various MPPT techniques on the basis of the properties such as tracking speed [7], complexity [12], MPP oscillation [13], accuracy and efficiency [14]. Reference [12] has compared many classical MPPT techniques based on array configuration, accuracy, cost of the system and tracking speed. However, [12] presents the application-based MPPTs which are not applicable

for every system. Reference [15] presents the comparison of various MPPT algorithms according to the PV application. Similarly, [16] also presents a review of many MPPT algorithms. The review is based on the control strategy, circuitry, and the application cost. This review reflects that the P&O is less complex with fast tracking capability amongst all algorithms presented. However, P&O is less accurate and consumes more power in MPPT during variable irradiances. Therefore, many modified P&O MPPT algorithms have been presented to overcome these problems. In this respect, [17] has proposed a modified P&O algorithm which resolves the drift problem during unpredicted irradiance change. As a result, this MPPT presents high efficiency and less power loss when tracking the operation point. Reference [18] has presented an adaptive P&O algorithm with predictive current control. However, it fails to consider the inductance change which influences the tracking accuracy of the algorithm. Similarly, [13] proposes a modified P&O algorithm with dynamic perturbation step size and a boundary condition to enhance the efficiency of the algorithm. Although this directs the system towards the operation point, it fails to handle the irradiance changes. Furthermore, [19] and [20] have proposed a dual-mode P&O algorithm with variable step-size, which resolves the problem of oscillation near the MPP and MPPT speed. However, the employed algorithm has a slightly higher cost compared with the traditional P&O, and is unable to identify the drift problem during variable irradiance condition. Hence, a modified MPPT technique needs to be proposed, which can resolve the aforementioned problems.

The issue of excess power generation during peak hours affects the distribution network. Therefore, it is required to limit the power transfer during peak hours. The power transfer is limited by introducing the tap-changing transformer and voltage regulator, increasing the conductor size, and using storage and curtailment approaches [5], [21]. Among all methods, the curtailment of surplus power is the most suitable [4]. In this respect, [6] has proposed a derated mode approach for curtailment of the surplus power. Likewise, various methods of derated mode operation are addressed in the literature. A current, voltage, power and P&O MPPT based derated power generation mode (DPGM) is implemented. P&O based DPGM is the most suitable due to less complexity. However, the system will have less efficiency and accuracy. Additionally, the algorithm oscillates near the operation point, i.e., drifting from the operation point in the random direction. Therefore, a novel MPPT algorithm is required to keep the system in DPGM with higher efficiency, accuracy, less drift, and the minimum power loss.

The significant contributions of this paper are summarized as follows.

1) A derated-mode GIPVS has been proposed to limit the power transfer and resolve the overvoltage problem at PCC during peak power generation.

2) The proposed scheme introduces a modified MPPT, which limits the power transfer.

3) This MPPT algorithm results in improved tracking speed and efficiency, which reduces the power loss under variable irradiance condition.

The remainder of the paper is organized as follows. Section II presents the system framework and its working strategy. Section III elaborates the proposed control strategy of GIPVS. Further, the simulation results are presented in Section IV to support the proposed control strategy. Finally, the conclusion is presented in Section V.

II. System Framwork and Working Strategy

This section briefs the system structure and proposed control strategy of GIPVS. The proposed system consists of two stages as shown in Fig. 1.

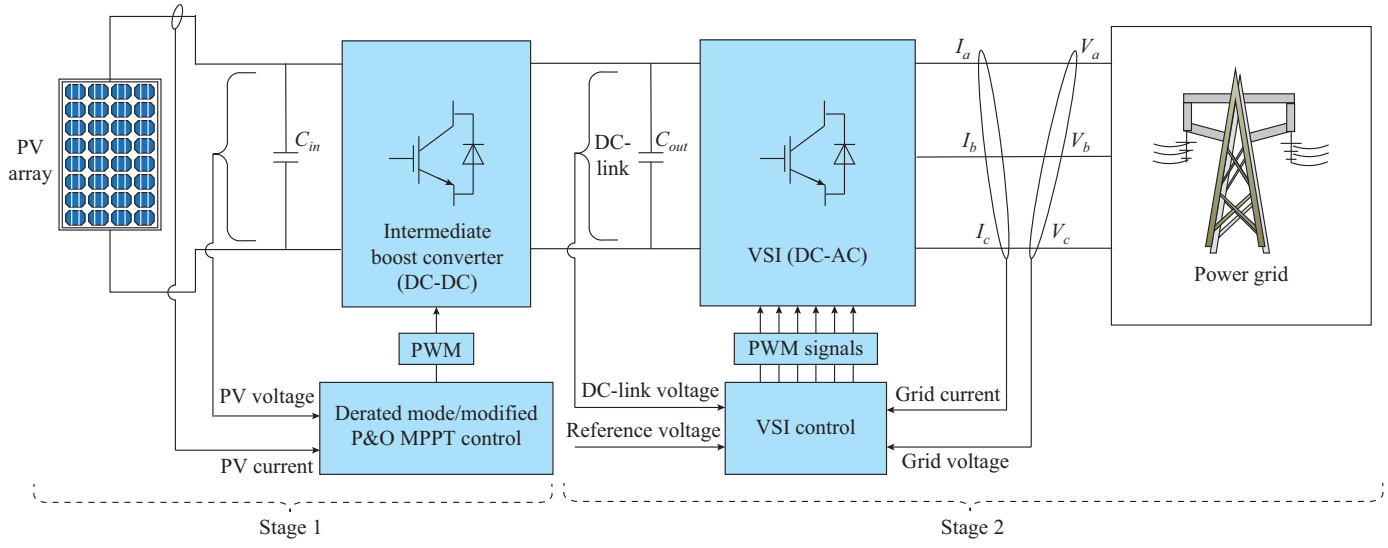

Fig. 1. Block diagram of proposed two-stage three-phase GIPVS.

Stage 1 includes a PV array, input capacitor C_{in}, boost converter, and the MPPT control. In the proposed system, a modified MPPT algorithm has been implemented which works in DPGM and modified MPPT mode. The DPGM

gets activated when the generation exceeds the pre-defined power limit P_{limit}; otherwise, it works in the modified MPPT mode [8]. Furthermore, the modified MPPT generates a pulse width modulation (PWM) signal for the boost converter to get a desired DC-link voltage level. On the other hand, Stage 2 is interfaced with DC-link capacitor C_{out}. Stage 2 consists of an insulated gate bipolar transistor (IGBT)-based voltage source inverter (VSI), and is integrated with the grid. The interfacing inductors are used between the inverter and the power grid to inject current as well as generated power with the help of inverter control. The inverter control of the proposed system is based on a dual control loop and the power grid synchronization technique. The control of the system is obtained in synchronously rotating or *dq* reference frame [22]. This consists of a direct (*d*) and quadrature (*q*) axis, which deals with the active and reactive power control, respectively. Furthermore, the controller generates the PWM signals to trigger the VSI and transfer power. Finally, the complete system is developed and simulated for a 30 kW two-stage three-phase GIPVS.

III. Proposed Control Technique

In this section, the control approach of each converter used for the first and second stage of the system has been presented. In the first stage, the functionality of MPPT with the boost converter is illustrated in the upcoming subsections.

A. Conventional P&O MPPT Algorithm

In the MPPT technique, the extracted voltage and current from the PV source are provided to the boost converter as shown in Fig. 2, where the inductor L_b, diode D_b, capacitor C_{PV}, and switch S_b are the designed components of the boost converter which provides the required voltage level with the MPPT controller.

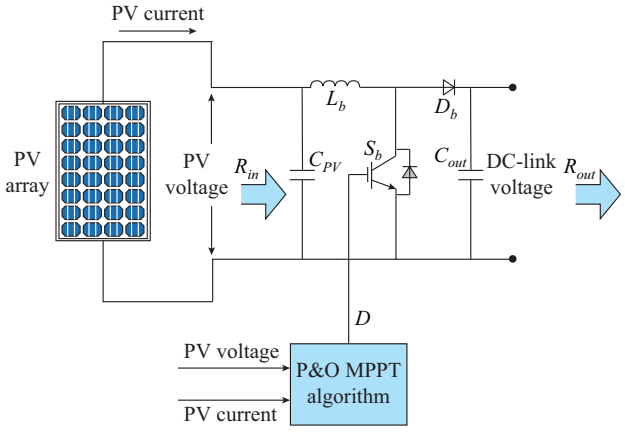

Fig. 2. Circuit diagram of DC-DC boost converter with MPPT control.

This controller reaches the operation point using direct duty ratio three-step strategy on the power-voltage (*P-V*) characteristic curve as shown in Fig. 3. $V_{PV}(k)$, $V_{PV}(k-1)$, and $V_{PV}(k+1)$ are the voltages of PV array at, before, and after the k^{th} instant, respectively; whereas the k^{th} instant defines the selected operation point on the *P-V* characteristic curve. The region of the operation point depends upon the slope of the power (change in PV power, i.e., ΔP_{PV}). The three-step approach is considered for the left and right operation regions of the *P-V* characteristic curve. In the left operation region, the slope of the power is positive with respect to the voltage, so it moves forward towards the operation point. In the right operation region, the power slope is negative with respect to the voltage, so it moves back towards the operation point as depicted below.

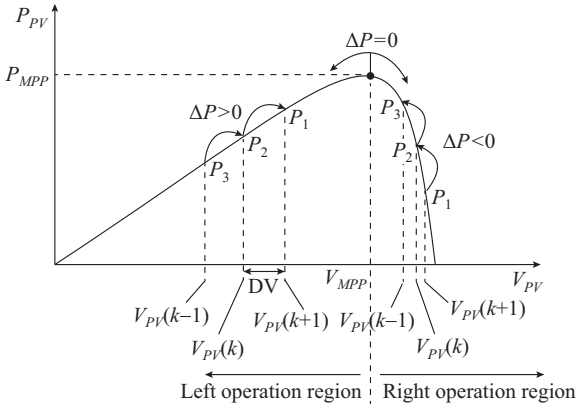

Fig. 3. Searching strategy of conventional P&O MPPT algorithm.

$$\begin{cases} \dfrac{dP_{PV}}{dV_{PV}} > 0 & \text{Move forwards towards MPP} \\ \dfrac{dP_{PV}}{dV_{PV}} < 0 & \text{Move back towards MPP} \\ \dfrac{dP_{PV}}{dV_{PV}} = 0 & \text{At MPP} \end{cases} \tag{1}$$

The corresponding increment and decrement in the duty ratio are due to the change of input power with respect to voltage. Consequently, the impact of the change in duty ratio on output voltage V_{DC} and current I_{DC} of boost converter can be illustrated as:

$$V_{DC} = \frac{1}{1-D} V_{PV} \tag{2}$$

$$I_{DC} = I_{PV}(1-D) \tag{3}$$

The ratio of V_{DC} and I_{DC} is the output impedance R_{out} of the boost converter which is calculated as:

$$R_{out} = \frac{V_{DC}}{I_{DC}} = \frac{R_{in}}{(1-D)^2} \tag{4}$$

At constant R_{in}, the value of R_{out} is inversely proportional to the duty ratio. Therefore, to achieve the maximum power, voltage and current at a particular duty ratio, the value of R_{out} is depicted as:

$$R_{out} = \frac{V_{MPP}}{I_{MPP}} \tag{5}$$

Moreover, the performance of P&O depends upon the increment or decrement in step size ΔD of the duty ratio [23]. The smaller the value of ΔD is, the longer the time response to achieve the MPP will be, which results in power loss. On the other hand, with a large step size, the response time is

short, but the drift problem occurs during the variable irradiance condition [17] due to the lack of knowledge of direction, i.e., an increase in ΔP_{PV} is due to variable irradiance or perturbation of ΔD. Therefore, it gets confusing for the operation point whether it should move towards or away from the MPP. Moreover, the conventional P&O only tracks the MPP during peak or non-peak hours of power generation. However, it does not participate in limiting the excess power generated during peak hours.

B. Modified P&O MPPT Algorithm

The proposed modified algorithm reduces the power loss and reduces the search time of MPP. It also keeps the system drift-free under variable irradiance condition. In addition, the proposed MPPT limits the excess power generation during peak hours. The proposed algorithm operates in two modes, i.e., modified MPPT mode and DPGM, which are illustrated in Fig. 4.

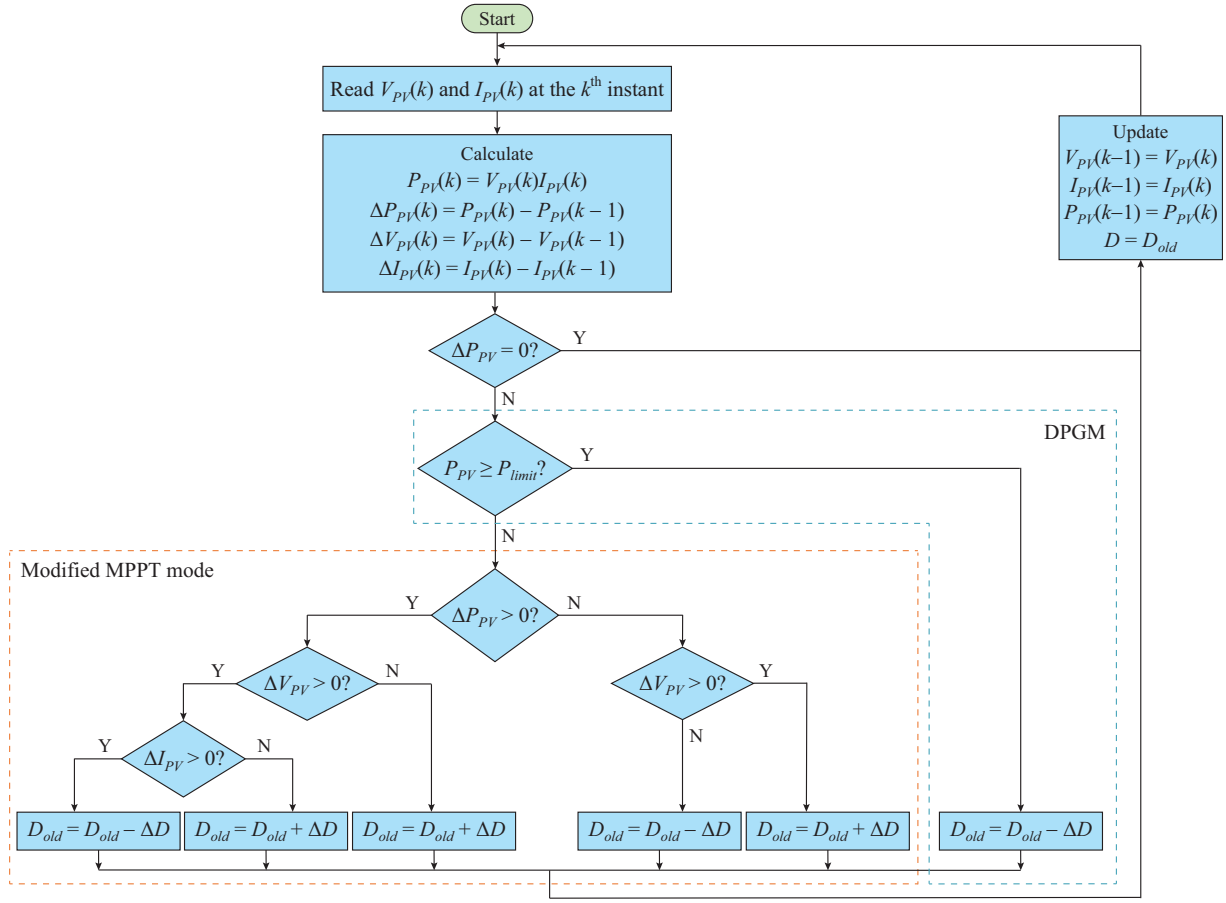

Fig. 4. Flow chart of modified P&O MPPT algorithm.

Whenever the generated PV power is within the power transfer limit, the system works in modified MPPT mode. Otherwise, the system works in DPGM as depicted below.

$$P_{DC}(t) = \begin{cases} P_{PV}(t) & \text{Modified MPPT mode for } P_{PV} < P_{limit} \\ P_{limit}(t) & \text{DPGM for } P_{PV} \geq P_{limit} \end{cases} \quad (6)$$

1) Modified MPPT Mode

The modified MPPT mode of the proposed algorithm follows the direct duty ratio D in a three-step strategy as mentioned in Section III-A. In the strategy, a large value of ΔD is considered for shorter response time. However, the large value of ΔD creates the problem of drift during irradiance change. As discussed in [17], the current level depends upon the irradiance level, which can be explained for a single diode model PV array, and the related equations are depicted as [24], [25]:

$$\begin{cases} I_{PV} = N_p \left[I_{sc} - I_o \left(\exp\left(\dfrac{V_{PV}}{N_s V_t} \right) - 1 \right) \right] \\ I_{sc} = N_p \left(I_{scn} + k_i (\Delta T) \right) \dfrac{G}{G_n} \end{cases} \quad (7)$$

The MPP value of the PV array delivered at particular R_{out} is depicted as:

$$I_{MPP} = N_p \left[I_{sc} - I_o \left(\exp\left(\frac{V_{MPP}}{N_s V_t} \right) - 1 \right) \right] \quad (8)$$

By using Taylor's expansion on (8) till the first order and substituting (4) and (5), (8) can be rewritten as:

$$V_{MPP} = \frac{N_p I_{sc}}{\dfrac{(1-D)^2}{R_{in}} + \dfrac{I_o N_p}{N_s V_t}} \quad (9)$$

$$I_{MPP}=\frac{(1-D)^2 N_p I_{sc}}{R_{in}\left[\frac{(1-D)^2}{R_{in}}+\frac{I_o N_p}{N_s V_t}\right]} \tag{10}$$

By substituting (7) into (9) and (10), V_{MPP} and I_{MPP} can be expressed as:

$$V_{MPP}=\frac{N_p^2\left(I_{scn}+k_i\Delta T\right)\frac{G}{G_n}}{\frac{(1-D)^2}{R_{in}}+\frac{I_o N_p}{N_s V_t}} \tag{11}$$

$$I_{MPP}=\frac{(1-D)^2 N_p^2\left(I_{scn}+k_i\Delta T\right)\frac{G}{G_n}}{R_{in}\left[\frac{(1-D)^2}{R_{in}}+\frac{I_o N_p}{N_s V_t}\right]} \tag{12}$$

Therefore, the maximum value of V_{MPP} and I_{MPP} with respect to G is expressed as:

$$\frac{\mathrm{d}V_{MPP}}{\mathrm{d}G}=\frac{N_p^2\left(\frac{I_{scn}+k_i\Delta T}{G_n}+\frac{G}{G_n}k_i\frac{\mathrm{d}T}{\mathrm{d}G}\right)}{\frac{(1-D)^2}{R_{in}}+\frac{I_o N_p}{N_s V_t}} \tag{13}$$

$$\frac{\mathrm{d}I_{MPP}}{\mathrm{d}G}=\frac{(1-D)^2 N_p^2\left(\frac{I_{scn}+k_i\Delta T}{G_n}+\frac{G}{G_n}k_i\frac{\mathrm{d}T}{\mathrm{d}G}\right)}{R_{in}\left[\frac{(1-D)^2}{R_{in}}+\frac{I_o N_p}{N_s V_t}\right]} \tag{14}$$

Since G is increasing, I_{scn}, I_o, k_i, N_p, N_s, V_t, and G_n are constants at STC, and G, D, and R_{in} are positive. Simultaneously, the temperature also increases with irradiance. Therefore, in (13) and (14), all terms are positive as the irradiance increases, which means that the voltage and current are positive with respect to irradiance, i. e., $\mathrm{d}V_{MPP}/\mathrm{d}G>0$ and $\mathrm{d}I_{MPP}/\mathrm{d}G>0$. Similarly, $\mathrm{d}V_{PV}/\mathrm{d}G>0$, and $\mathrm{d}I_{PV}/\mathrm{d}G>0$.

Thus, based on current, voltage and power information, the drift problem can be avoided and analyzed as follows.

When the irradiance is increasing, point b shifts to point c and then to point d on a new P-V curve, as shown in Fig. 5.

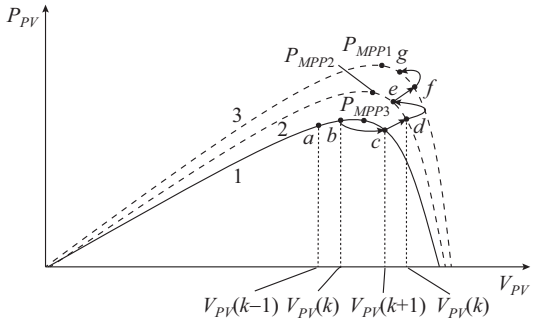

Fig. 5. Drift analysis of operation point during variable irradiance condition.

On this curve, the differences between points b and d for P, V, and I are positive. It can be observed that the ΔV and ΔI are positive only when the irradiance is increasing. This shows that the current information during MPPT is essential. Further, based on these observations, ΔV and ΔI are positive, which leads to the reduction in the duty ratio. Consequently, the corresponding voltage decreases compared with the conventional P&O, where the voltage increases. This means that the operation point which is used to move away from the MPP starts moving towards the MPP because of the current information. It means that the operation point is not deviating from the MPP during variable irradiance condition, or, in other words, not drifting away from the MPP.

2) DPGM

In DPGM, the modified P&O MPPT algorithm gets activated during available surplus power. As we know, the peak power rating of the installed PV array is always more than the average power generated in the whole day. Thus, the PV array generates surplus power during peak hours. Therefore, to remove the surplus power, a power limit is required so that the power can be transferred without affecting the distribution network equipment. In this paper, a power limit P_{limit} has been considered which is the average of power generated during 9 to 16 hours and is presented as:

$$P_{limit}(t)=\frac{P(t_9)+P(t_{10})+\ldots+P(t_{16})}{t_9+t_{10}+\ldots+t_{16}} \tag{15}$$

When the generated power exceeds P_{limit}, the DPGM turns on and shaves the surplus power. In Fig. 6, the power curve is within the limit at every time instant (i. e., not reaching the maximum generated power P_{peak}), which shows the active participation of DPGM.

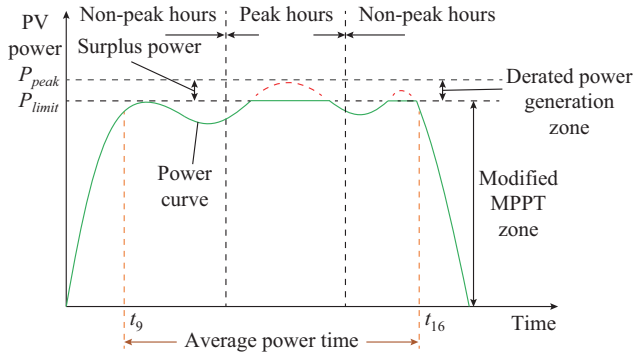

Fig. 6. Day-time power profile of a PV array.

Based on the above discussion in Sections III-A and III-B, the conventional and proposed MPPT algorithms with boost converter generate the DC power in the first stage. Furthermore, in the second stage, the generated DC power is provided to the VSI for power conversion with inverter control which has been discussed in the previous subsection.

C. Inverter Control for Grid Integration

The generated DC power is converted into AC power using VSI. The obtained AC power is further injected into the power grid with the help of inverter control as shown in Fig. 7. In this process, the inverter control performs voltage regulation, current control and grid synchronization in synchronous dq reference frame. The voltage regulation or outer

loop produces the reference current I_d^*. In this loop, the DC-link voltage is compared with a pre-defined reference voltage using a proportional-integral (PI) controller which produces I_d^* as shown in Fig. 8. On the other hand, in the inner loop, the decoupled current control scheme is used to generate the gate pulses for the VSI. In this technique, I_d^* is taken as the reference current for the active power control. Similarly, I_q^* is the reference current for reactive power control, which is set to be zero for transfering power at unity power factor. Furthermore, both active and reactive power controllers generate the modulating signals as shown in Fig. 9. The respective mathematical modelling of the system in Fig. 7 is depicted below [26].

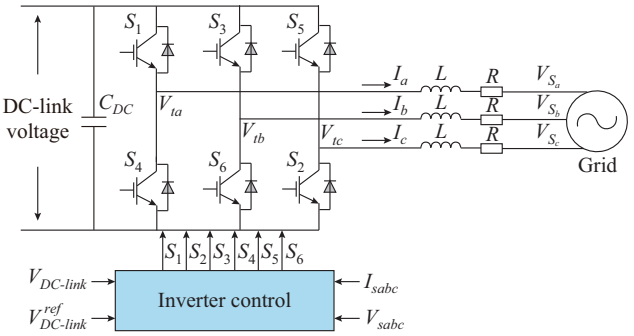

Fig. 7. Circuit diagram of grid-integrated VSI.

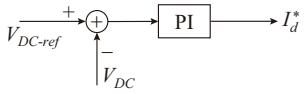

Fig. 8. Voltage regulation/outer loop of inverter control.

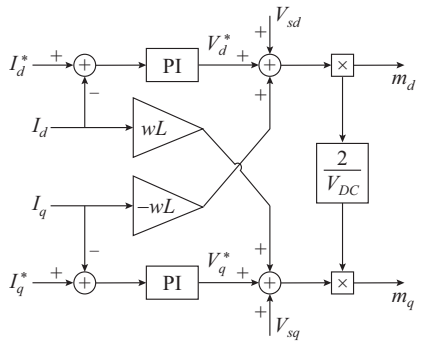

Fig. 9. Current control/inner loop of inverter control.

$$\frac{\mathrm{d}I_i}{\mathrm{d}t} = -\frac{R}{L} I_i + \frac{1}{L}(V_{ti} - V_{si}) \quad i = a, b, c \tag{16}$$

The mathematical expressions of the system are of a higher degree in the natural reference frame (*abc*). Therefore, to use a simple controller (i.e., PI) and realize less mathematical complexity, the present reference frame *abc* is transformed into rotating reference frame *dq* using Park's transform [27], and the resultant equations are illustrated as:

$$\begin{cases} \dfrac{\mathrm{d}I_d}{\mathrm{d}t} = -\dfrac{R}{L} I_d \pm \omega I_q + \dfrac{1}{L}(V_{td} - V_{sd}) \\ \dfrac{\mathrm{d}I_q}{\mathrm{d}t} = -\dfrac{R}{L} I_q \pm \omega I_d + \dfrac{1}{L}(V_{tq} - V_{sq}) \end{cases} \tag{17}$$

Or:

$$L\frac{\mathrm{d}I_i}{\mathrm{d}t} = -RI_i + V_i^* \quad i = d, q \tag{18}$$

$$\begin{cases} V_d^* = V_{td} - V_{sd} \pm \omega L I_q \\ V_q^* = V_{tq} - V_{sq} \pm \omega L I_d \end{cases} \tag{19}$$

As mentioned in [28], the terminal voltage of inverter requires input DC-link voltage and modulation index. Hence, in *dq*-reference frame, the modulation index is presented as:

$$V_{ti} = m_i \frac{V_{DC}}{2} \quad i = d, q \tag{20}$$

By substituting (20) into (19), the modulating signals are:

$$\begin{cases} m_d = \dfrac{2}{V_{DC}}(V_d^* \mp \omega L I_q + V_{sd}) \\ m_q = \dfrac{2}{V_{DC}}(V_q^* \mp \omega L I_d + V_{sq}) \end{cases} \tag{21}$$

These modulating signals m_d and m_q have been transformed from *dq* to *abc* to provide the gate signals (S_1-S_6) to the VSI, which generates voltage and current. Since the power has to be transferred in the grid, the generated voltage and current should be in phase. Thus, a phase-locked loop technique has been added in the system, which synchronizes the generated voltage of VSI and the current with the power grid.

Finally, in the next section, the performance of the control approaches will be evaluated and verified in MATLAB/Simulink environment.

IV. Simulation Results

A 30 kW two-stage three-phase GIPVS using modified P&O MPPT algorithm is simulated in MATLAB/Simulink environment with Simpower tools. The modified MPPT performs derated power generation which restricts the power generation when it exceeds P_{limit}. Simultaneously, the conventional P&O algorithm is also examined to select a suitable ΔD for the modified P&O algorithm under variable irradiance condition. Thereafter, the performance of the conventional and modified P&O algorithm are analysed in terms of PV power, PV voltage, duty ratio, DC-link and output power as follows.

A. Conventional P&O MPPT Algorithm

For the evaluation of input voltage deviation and response time, the conventional P&O algorithm is tested for different values of ΔD. Simultaneously, to test the robustness of the system, the algorithm is evaluated under variable irradiance condition. For the sake of evaluation, a small step size $\Delta D = 3\times10^{-7}$ and a big step size $\Delta D = 3\times10^{-4}$ are considered. From Fig. 10(a) and (b), due to the large step size, the oscillation in input voltage is significant. Furthermore, it is evident that the duty ratio achieves a steady-state condition in less time under variable irradiance condition, which is shown in Fig. 10. Hence, it can be concluded that the fast dynamic response can be achieved through a large step size. However, the operation point oscillates near the MPP due to large step size. To remove the oscillation near the MPP, a modified P&O algorithm is adopted.

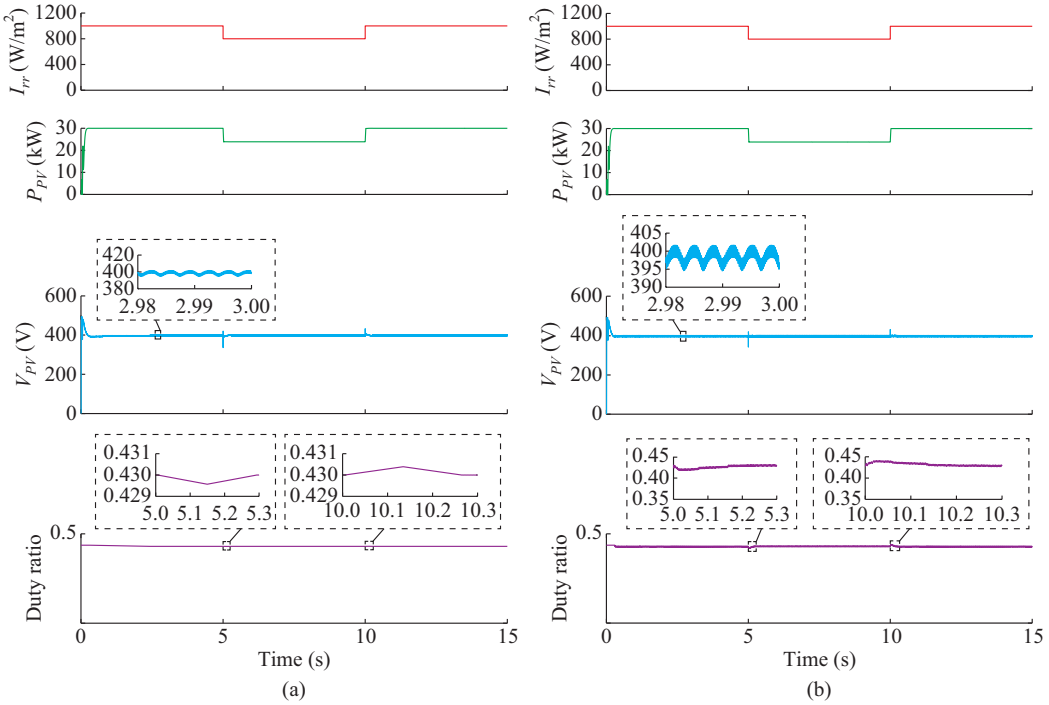

Fig. 10. Steady state performance of conventional P&O algorithm. (a) At $\Delta D = 3 \times 10^{-7}$. (b) At $\Delta D = 3 \times 10^{-4}$.

B. Modified P&O MPPT Algorithm

The performance of the modified P&O algorithm is evaluated in two modes. One is the modified MPPT mode and the other is the DPGM.

1) Modified MPPT Mode

In this mode, the modified MPPT works like the conventional P&O until the power generation does not reach the power limit. Besides, the modified algorithm provides the right direction and less variation in voltage of the operation point towards MPP. Figure 11(a) depicts the variation in V_{PV}, which is less compared with the conventional P&O algorithm. Simultaneously, the change in the duty ratio is positive when irradiance is increasing as discussed in the modified MPPT mode of Section III. On the other hand, when irradiance is decreasing, the current decreases, so the input voltage and the corresponding duty ratio increase.

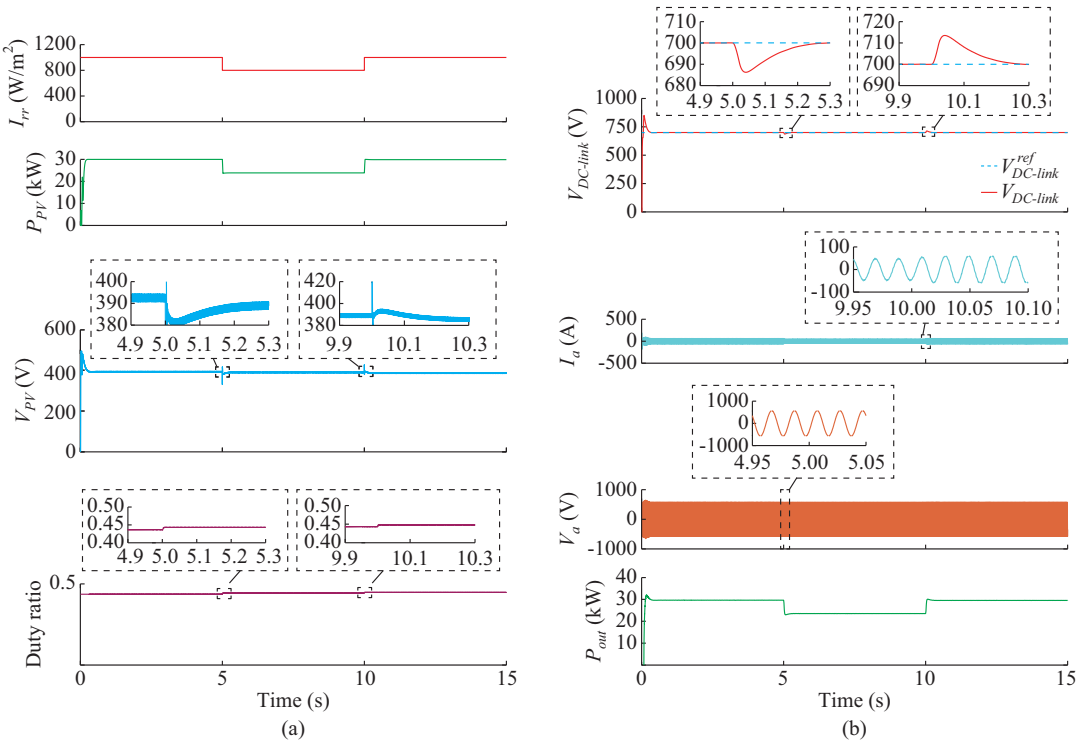

Fig. 11. Dynamic performance of modified P&O algorithm in modified MPPT mode. (a) PV source output performance. (b) DC-link and inverter output performance.

Thus, V_{PV} does not deviate and reaches the operation point. In addition, the effect of irradiance change in DC-link voltage, phase voltage V_a, and current I_a is shown in Fig. 11(b).

2) DPGM

The system enters into the DPGM when the net power generation exceeds the power limit. In this mode, the modified P&O MPPT algorithm curtails the excess power. A power profile is presented in Fig. 6 which is based on the irradiance change in a day. In this paper, the system is simulated for $t=15$ s, where one second is scaled as one hour of the day to replicate the peak and non-peak hours of the power profile. Figure 12(a) depicts that the system starts generating power from $t=0$ and it enters into the peak-hour zone after $t=5$ s. In this zone, the excess power is shaved using modified MPPT, and remains in this mode till $t=9$ s. During this time, the system generates P_{limit} of 24 kW, which is the average power during 9 to 16 hours. The system performs in the DPGM. Furthermore, the performance of V_{PV}, duty ratio, DC-link voltage, grid voltage, and current are presented in Fig. 12(b).

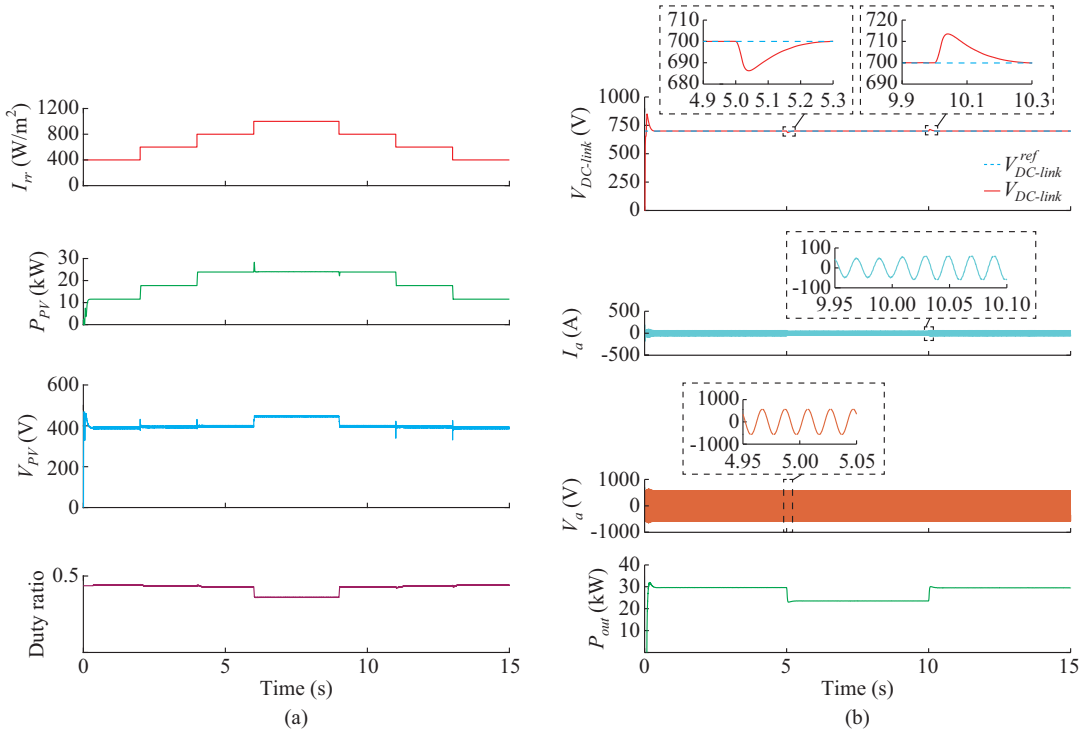

Fig. 12. Dynamic performance of modified P&O algorithm in DPGM. (a) PV source output performance. (b) DC-link and inverter output performance.

C. Statical Analysis

Further, to analyze the performance of proposed modified and conventional P&O MPPT algorithms, a statical analysis has been presented in Table I, where SD is the standard deviation. The statical analysis is presented in terms of mean and SD of the settling time to meet V_{MPP} and $V_{DC\text{-}link}^{ref}$ of the system. In this respect, 30 trial runs are carried out to analyze the performance of both the algorithms under constant and variable irradiance conditions. The trial runs are performed under constant irradiance condition, i.e., 600 W/m^2 for $t=6$ s. Whereas under variable irradiance condition at $t=1.5$ s, it changes from 600 W/m^2 to 400 W/m^2 and back from 400 W/m^2 to 600 W/m^2 at $t=3$ s. In Table I, the mean and SD of the settling time are summarized for the outcome of all 30 trials. The mean result of the proposed algorithm is better than the conventional algorithm. Simultaneously, the SD results of the proposed algorithm are almost zero under constant and variable irradiance conditions. The aforementioned results indicate the high robustness and search capability of the proposed modified P&O algorithm.

TABLE I
PERFORMANCE ANALYSIS OF MODIFIED AND CONVENTIONAL P&O MPPT ALGORITHMS

No.	Irradiance condition	Evaluation parameter	Mean or SD	Conventional P&O	Modified P&O
1	Under constant irradiance condition (600 W/m^2)	$t_{s,V_{MPP}}$	Mean	0.768	0.61
			SD	2.2781×10^{-16}	1.1391×10^{-16}
		$t_{s,V_{DC\text{-}link}^{ref}}$	Mean	0.6312	0.57
			SD	0.000410391	1.13906×10^{-16}
2	Under variable irradiance condition (600 to 400 W/m^2)	$t_{s,V_{MPP}}$	Mean	1.9365	1.768
			SD	0.03437793	0.00615587
		$t_{s,V_{DC\text{-}link}^{ref}}$	Mean	2.066	2.049
			SD	0	0.003077935
3	Under variable irradiance condition (400 to 600 W/m^2)	$t_{s,V_{MPP}}$	Mean	3.265	3.237
			SD	4.55626×10^{-16}	0.03785012
		$t_{s,V_{DC\text{-}link}^{ref}}$	Mean	3.5319	3.39
			SD	0.004278465	4.55626×10^{-16}

V. Conclusion

A two-stage three-phase GIPVS works in the DPGM to curtail the extra feed-in power during peak hours. In addition, it avoids the drift phenomena which exists in traditional P&O algorithm. Furthermore, the proposed algorithm works in a modified MPPT mode during non-peak hours. In this mode, the MPPT holds the information of current to distinguish irradiance change. Thus, it can estimate the search direction towards MPP during irradiance change. Thereby, the operation point does not diverge from the shortest path of MPPT. Moreover, to enhance the tracking capability of the modified MPPT, it is examined on different step sizes ΔD. In this paper, a large step size has been chosen which increases the response time and reduces the oscillation using the proposed algorithm. The system is implemented for a 30 kW two-stage three-phase GIPVS and simulated in MATLAB/Simulink environment using Simpower tools. The performance of the system presents that the proposed algorithm actively participates in power curtailment during peak hours of power generation. Additionally, the performance shows that the modified algorithm gives a faster response than the traditional P&O algorithm under variable irradiance condition.

References

[1] O. Abedinia, D. Raisz, and N. Amjady, "Effective prediction model for hungarian small-scale solar power output," *IET Renewable Power Generation*, vol. 11, no. 13, pp. 1648-1658, Nov. 2017.

[2] O. Abedinia, N. Amjady, and N. Ghadimi, "Solar energy forecasting based on hybrid neural network and improved metaheuristic algorithm," *Computational Intelligence*, vol. 34, no. 1, pp. 241-260, Feb. 2018.

[3] F. Blaabjerg, Z. Chen, and S. B. Kjaer, "Power electronics as efficient interface in dispersed power generation systems," *IEEE Transactions on Power Electronics*, vol. 19, no. 5, pp. 1184-1194, Sept. 2004.

[4] Q. Zhou and J. W. Bialek, "Generation curtailment to manage voltage constraints in distribution networks," *IET Generation, Transmission & Distribution*, vol. 1, no. 3, pp. 492-498, May 2007.

[5] R. Tonkoski, L. A. C. Lopes, and T. H. M. El-Fouly, "Coordinated active power curtailment of grid connected PV inverters for overvoltage prevention," *IEEE Transactions on Sustainable Energy*, vol. 2, no. 2, pp. 139-147, Apr. 2011.

[6] W. A. Omran, M. Kazerani, and M. M. A. Salama, "Investigation of methods for reduction of power fluctuations generated from large grid-connected photovoltaic systems," *IEEE Transactions on Energy Conversion*, vol. 26, no. 1, pp. 318-327, Mar. 2011.

[7] A. Ahmed, L. Ran, S. Moon *et al.*, "A fast PV power tracking control algorithm with reduced power mode," *IEEE Transactions on Energy Conversion*, vol. 28, no. 3, pp. 565-575, Sept. 2013.

[8] Y. Yang, H. Wang, F. Blaabjerg *et al.*, "A hybrid power control concept for PV inverters with reduced thermal loading," *IEEE Transactions on Power Electronics*, vol. 29, pp. 6271-6275, no. 12, Dec. 2014.

[9] A. Sangwongwanich, Y. Yang, and F. Blaabjerg, "High-performance constant power generation in grid-connected PV systems," *IEEE Transactions on Power Electronics*, vol. 31, no. 3, pp. 1822-1825, Mar. 2016.

[10] A. Sangwongwanich, Y. Yang, F. Blaabjerg *et al.*, "Benchmarking of constant power generation strategies for single-phase grid-connected photovoltaic systems," *IEEE Transactions on Industry Applications*, vol. 54, no. 1, pp. 447-457, Jan. 2018.

[11] H. D. Tafti, A. I. Maswood, G. Konstantinou *et al.*, "A general constant power generation algorithm for photovoltaic systems," *IEEE Transactions on Power Electronics*, vol. 33, no. 5, pp. 4088-4101, May 2018.

[12] S. Jain and V. Agarwal, "Comparison of the performance of maximum power point tracking schemes applied to single-stage grid-connected photovoltaic systems," *IET Electric Power Applications*, vol. 1, no. 5, pp. 753-762, Sept. 2007.

[13] Z. Salam and J. Ahmed, "A modified P&O maximum power point tracking method with reduced steady-state oscillation and improved tracking efficiency," *IEEE Transactions on Sustainable Energy*, vol. 7, no. 4, pp. 1506-1515, Oct. 2016.

[14] L. Zhang, S. S. Yu, T. Fernando *et al.*, "An online maximum power point capturing technique for high-efficiency power generation of solar photovoltaic systems," *Journal of Modern Power Systems and Clean Energy*, vol. 7, no. 2, pp. 357-368, Mar. 2019.

[15] T. Esram and P. L. Chapman, "Comparison of photovoltaic array maximum power point tracking techniques," *IEEE Transactions on Energy Conversion*, vol. 22, no. 2, pp. 439-449, Jun. 2007.

[16] B. Subudhi and R. Pradhan, "A comparative study on maximum power point tracking techniques for photovoltaic power systems," *IEEE Transactions on Sustainable Energy*, vol. 4, no. 1, pp. 89-98, Jan. 2013.

[17] M. Killi and S. Samanta, "Modified perturb and observe MPPT algorithm for drift avoidance in photovoltaic systems," *IEEE Transactions on Industrial Electronics*, vol. 62, no. 9, pp. 5549-5559, Sept. 2015.

[18] Y. Yang and H. Wen, "Adaptive perturb and observe maximum power point tracking with current predictive and decoupled power control for grid-connected photovoltaic inverters," *Journal of Modern Power Systems and Clean Energy*, vol. 7, no. 2, pp. 422-432, Mar. 2019.

[19] F. Liu, S. Duan, F. Liu *et al.*, "A variable step size INC MPPT method for PV systems," *IEEE Transactions on Industrial Electronics*, vol. 55, no. 7, pp. 2622-2628, Jul. 2008.

[20] A. Ghamrawi, J.-P. Gaubert, and D. Mehdi, "A new dual-mode maximum power point tracking algorithm based on the perturb and observe algorithm used on solar energy system," *Solar Energy*, vol. 174, no. 1, pp. 508-514, Nov. 2018.

[21] F. Olivier, P. Aristidou, D. Ernst *et al.*, "Active management of low-voltage networks for mitigating overvoltages due to photovoltaic units," *IEEE Transactions on Smart Grid*, vol. 7, no. 2, pp. 926-936, Mar. 2016.

[22] M. Shayestegan, "Overview of grid-connected two-stage transformerless inverter design," *Journal of Modern Power Systems and Clean Energy*, vol. 6, no. 4, pp. 642-655, Jul. 2018.

[23] A. I. Ali, M. A. Sayed, and E. E. Mohamed, "Modified efficient perturb and observe maximum power point tracking technique for grid-tied PV system," *International Journal of Electrical Power & Energy Systems*, vol. 99, pp. 192-202, Jul. 2018.

[24] A. Ramyar, H. Iman-Eini, and S. Farhangi, "Global maximum power point tracking method for photovoltaic arrays under partial shading conditions," *IEEE Transactions on Industrial Electronics*, vol. 64, no. 4, pp. 2855-2864, Apr. 2017.

[25] S. Liu, P. X. Liu, and X. Wang, "Stochastic small-signal stability analysis of grid-connected photovoltaic systems," *IEEE Transactions on Industrial Electronics*, vol. 63, no. 2, pp. 1027-1038, Feb. 2016.

[26] V. Kumar and M. Singh, "Sensorless DC-link control approach for three-phase grid integrated PV system," *International Journal of Electrical Power & Energy Systems*, vol. 112, pp. 309-318, Nov. 2019.

[27] X. Wang, F. Zhuo, J. Li *et al*., "Modeling and control of dual-stage high-power multifunctional PV system in *d-q*-coordinate," *IEEE Transactions on Industrial Electronics*, vol. 60, no. 4, pp. 1556-1570, Apr. 2013.

[28] A. K. Singh, I. Hussain, and B. Singh, "Double-stage three-phase grid-integrated solar PV system with fast zero attracting normalized least mean fourth based adaptive control," *IEEE Transactions on Industrial Electronics*, vol. 65, no. 5, pp. 3921-3931, May 2018.

Vinit Kumar received the B.Tech. degree in electrical and electronic engineering from Rajasthan Technical University, Kota, India, in 2012, and the M.E. degree in power system from the Thapar Institute of Engineering and Technology, Patiala, India, in 2015, where he is currently working toward the Ph.D. degree at the Department of Electrical and Instrumentation Engineering. His research interests include grid-interfaced converters, PV systems, and grid integration of renewable energy sources.

Mukesh Singh received the B.Tech. degree in electrical engineering from BIT, Sindhri, India, in 2000, the M.E. degree in electrical engineering from the Walchand College of Engineering, Sangli, India, in 2008, and the Ph.D. degree from Indian Institute of Technology, Guwahati, India, in 2013. He is currently working as Associate Professor with the Department of Electrical and Instrumentation Engineering, Thapar Institute of Engineering and Technology, Patiala, India. His research interests include smart grid, electric vehicle, renewable energy sources and distributed generation.